Promoting electrocatalytic nitrogen reduction to ammonia via Fe-boosting nitrogen activation on MnO_2 surfaces

Ting Huang,[a,1] Zaichun Liu,[b,1] Yu Zhang,[a] Faxing Wang,[c] Juan Wen,[b] Chengyin Wang,[d] Masud Hossain,[b] Qingji Xie,[a,*] Shouzhuo Yao,[a,*] Yuping Wu[b,*]

[a] Key Laboratory of Chemical Biology & Traditional Chinese Medicine Research (Ministry of Education of China), College of Chemistry and Chemical Engineering, Hunan Normal University, Changsha 410081, Hunan, China

[b] School of Energy Science and Engineering & Institute of Advanced Materials, Nanjing Tech University, Nanjing 211816, Jiangsu Province, China

[c] Department of Chemistry and Food Chemistry & Center for Advancing Electronics Dresden (cfaed), Technische Universität Dresden, 01062, Dresden, German

[d] College of Chemistry & Chemical Engineering, Yangzhou University, Yangzhou 225127, Jiangsu Province, China

Electronic supporting information (ESI):

Material

$KMnO_4$, sodium salicylate ($C_7H_5O_3Na$), sodium hypochlorite (NaClO), $Na_2[Fe(CN)_5NO]\cdot 2H_2O$, ethanol were purchased from Macklin Biochemical Co., Ltd (Shanghai, China). Sodium sulfate, iron nitrate, sodium hydroxide, potassium chloride were purchased from Sinopharm Chemical Reagent Co., Ltd (Shanghai, China). The ultrapure water used throughout all experiments was purified through a Millipore system.

Ammonia detection

1) Oxidizing agent: 0.75 M NaOH and NaClO (4.5%, Active chlorine).
2) Coloring agent: 0.32 M NaOH and 0.4 M $C_7H_5O_3Na$.
3) Catalyst agent: 1 g $Na_2Fe(CN)_5NO\cdot 2H_2O$ diluted to 10 mL with deionized water.
4) Standard solution: NH_4Cl with a serious of concentrations.

Concentration of produced NH_3 was determined by UV–vis absorption spectra with indophenol blue.[1] Specifically, 4 mL of the electrolyte was taken from the cathode chamber. Then 50 μL of oxidizing agent, 500 μL of coloring agent and 50 μL of catalyst agent were added into the above electrolyte in turn. After standing at room temperature for 2 h in dark, the absorption spectra of the resulting solution were measured with an ultraviolet-visible (UV-vis) spectrophotometer. The formed indophenol blue was determined by absorbance at 660 nm. The concentration-absorbance curves were calibrated using standard NH_4Cl solution with NH_3 concentrations of 0.0, 0.05, 0.1, 0.15, 0.2, 0.25, 0.3, 0.4, 0.5, 0.6, 0.7, 0.8, 0.9, 1.0 μg mL^{-1} in 0.1 M Na_2SO_4. The fitting curve ($y = 0.4409x + 0.0539$, $R^2 = 0.999$) indicates good linear relation of absorbance value with NH_3 concentration by three times independent calibrations.

Hydrazine detection

The amount of hydrazine in electrolyte was measured by the method of Watt and Chrisp.[2] In detail, 5 mL of the electrolyte solution was taken out and then mixed with 5 mL of the coloring solution (a mixture of 5.99 g para-(dimethylamino) benzaldehyde, 30 mL concentrated HCl and 300 mL ethanol). The absorbance of resulting solution was measured at a wavelength of 455 nm. The concentration-absorbance curves were calibrated using standard $N_2H_4 \cdot H_2O$ solution in a series of concentrations. The fitting curve ($y = 0.8949x + 0.01$, $R^2 = 0.9998$) shows a good

linear relation between absorbance with N_2H_4 concentration in three independent calibrations.

Determination of NH_3 yield and FE

The Faradaic efficiency for N_2 reduction was defined as the amount of electric charge used for synthesizing NH_3 divided the total charge passed through the electrodes during the electrolysis. The total amount of NH_3 produced was measured using colorimetric methods. Assuming three electrons were needed to produce one NH_3 molecule, the FE could be calculated as follows

$$FE = 3 \times F \times C_{NH3} \times V / (17 \times Q) \times 100\% \quad \text{(S1)}$$

The v_{NH3} was calculated using the following equation

$$v_{NH3} = C_{NH3} \times V / (m_{cat.} \times t) \text{ or } v_{NH3} = C_{NH3} \times V / (17 \times A \times t) \quad \text{(S2)}$$

where F is the Faraday constant, C_{NH3} is the measured molar concentration of NH_4^+, V is the electrolyte volume, Q is the total quantity of applied electricity, m is the mass of the catalyst or active component, t is the reaction time, and A is the geometric area.

Computational Details

First-principles calculations were performed with the generalized gradient approximation (GGA)[3] in the form of the Perdew, Burke, and Ernzerhof (PBE)[4] exchange-correlation functional, as implemented in the Dmol^3 package.[5] An eight atom layers MnO_2 (211) surface was modeled for Fe-substitution with 20 Å vacuum space to avoid the interaction form nearby layers. Layers 5 to 8 are central layers and 1 to 4 are surface layers. One Mn atom from the surface of MnO_2 (211) was replaced by a Fe atom, named as Fe-MnO_2. Structural relaxation was performed until the convergence criteria for energy were set to be 10^{-5} eV, and 0.002 Ha Å^{-1} was adopted for the total energy calculations. The Brillouin zone integration was performed with 2 × 2 × 1 Γ-centred Monkhorst-Pack k-point meshes in geometry optimization. The N_2 adsorption energy is defined as:

$$E_{ads} = E_{N_2/substrate} - E_{substrate} - E_{N2} \quad \text{(S3)}$$

After the geometry optimization, frequencies of each complex were calculated and the free energy was obtained as follows:

$$\Delta G=\Delta E+\Delta ZPE-T\Delta S+\Delta Gu+\Delta GpH \quad (S4)$$

where ΔE, ΔZPE and ΔS represent the change in calculated total energy, zero-point energy and entropy between the products and reactants, respectively. T represents the temperature (298.15 K). ΔGU = −neU, where n represents the number of transferred charge, and U represents the electrode potential with respect to the normal hydrogen electrode. ΔG_{pH} represents the correction H^+ free energy by the concentration, which can be calculated through ΔGpH = 0.059×pH (the value of pH is assumed to be zero in this work).

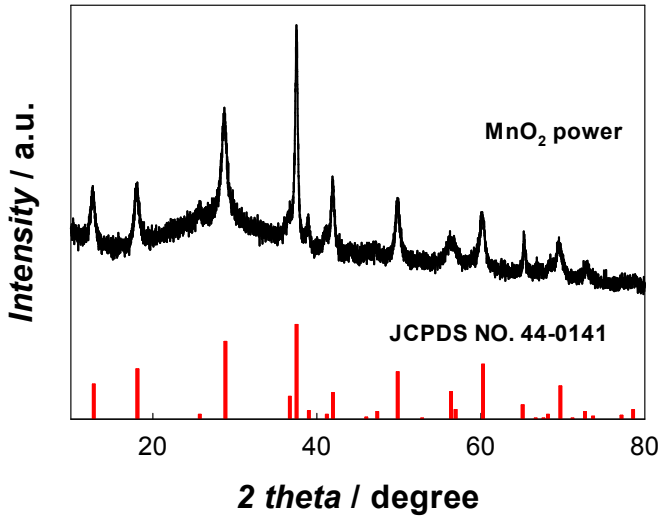

Fig. S1 XRD patterns of MnO_2.

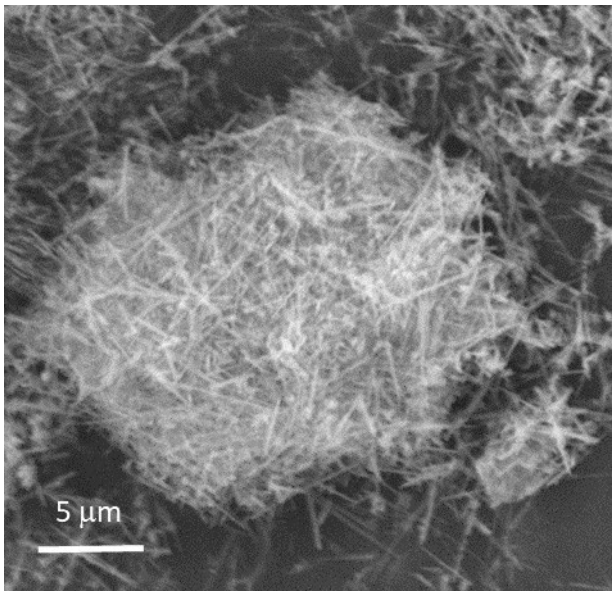

Fig. S2 SEM image of MnO_2.

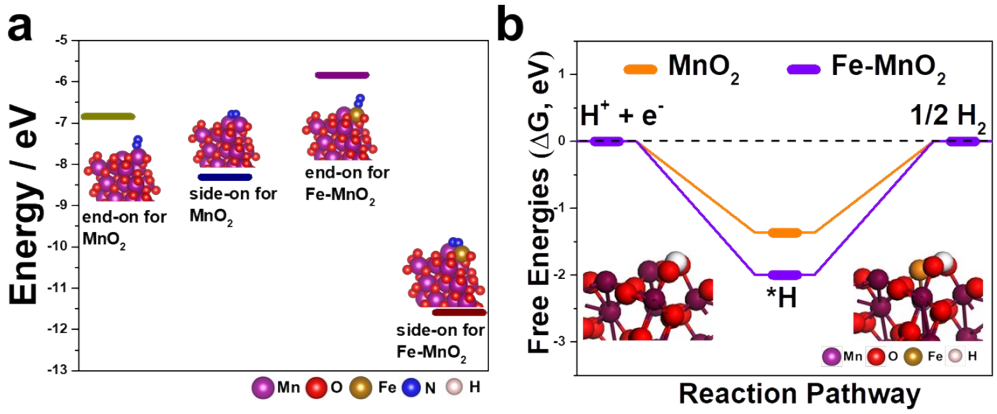

Fig. S3 (a) DFT-calculated adsorption energies of N_2 adsorption on (211) surface of MnO_2 and Fe-MnO_2 for side-on and end-on configurations. (b) DFT-calculated free energy pathways of HER on (211) surface of MnO_2 and Fe-MnO_2 at surface potential of 0 V under 298.15 K. Insets are the corresponding optimized atomic structures.

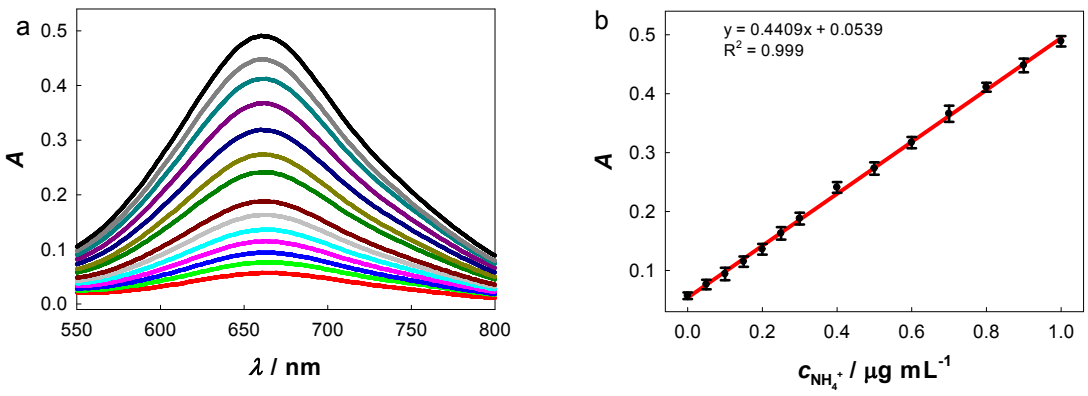

Fig. S4 (a) UV-Vis spectra of various NH_4^+ concentrations (mother solution: 0.1 M Na_2SO_4) after incubated for 2 h at room temperature. (b) Calibration curve used for calculation of NH_3 concentrations.

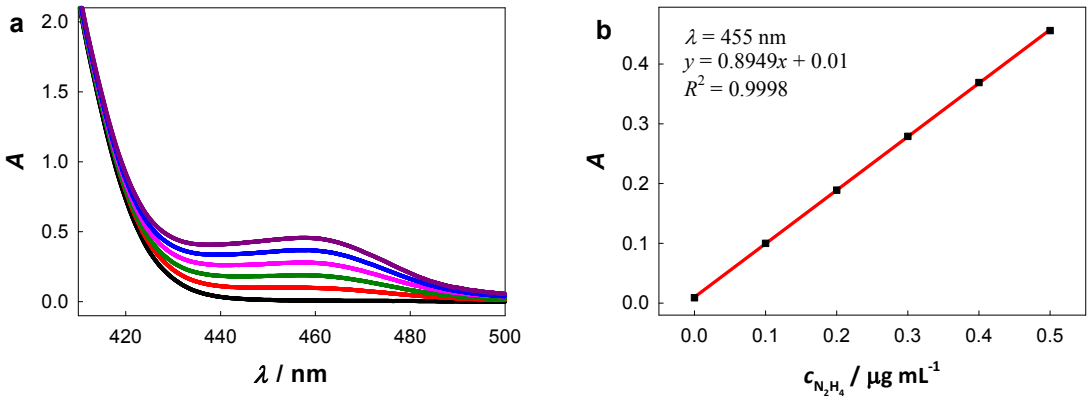

Fig. S5 (a) UV-Vis absorption spectra of various N_2H_4 concentrations after incubated for 30 min at room temperature. (b) Calibration curve used for estimation of N_2H_4 concentration.

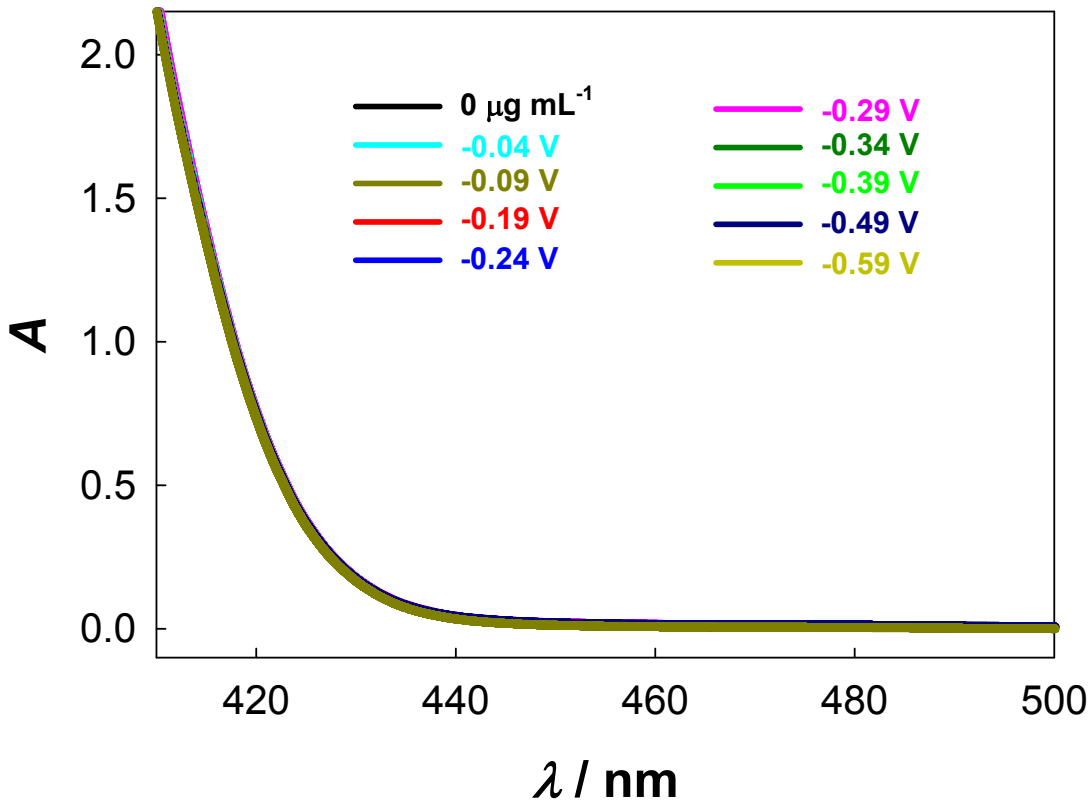

Fig. S6 UV–Vis spectra of the electrolyte estimated by the method of Watt and Chrisp after 2 h electrolysis at a series of potentials under ambient conditions.

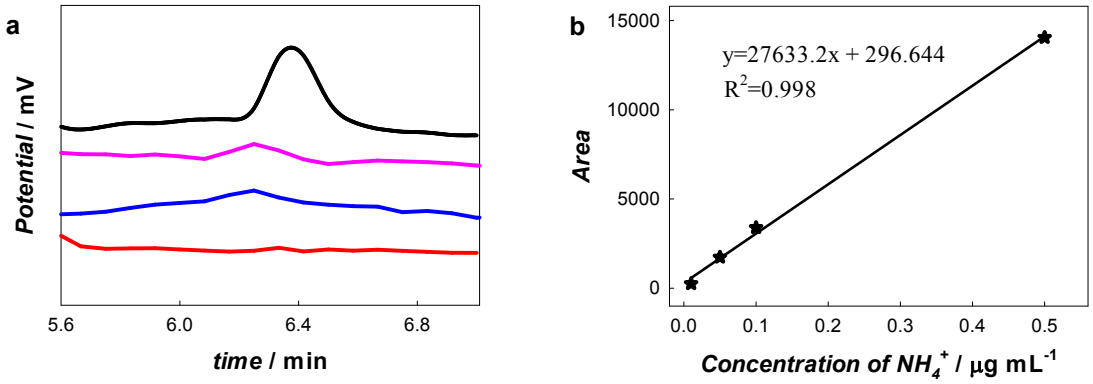

Fig. S7 (a) Ion chromatogram spectra of the standard NH_4^+ concentrations. (b) Calibration curve used for calculation of NH_4^+ concentrations.

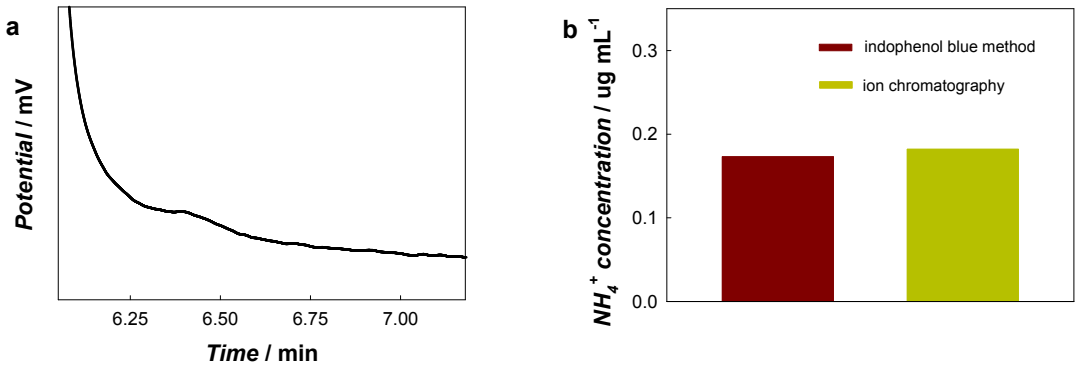

Fig. S8 (a) Ion chromatograms for NRR with Fe–MnO_2 at -0.29 V after electrolysis. (b) NH_4^+ concentration of Fe–MnO_2 at -0.29 V after 2 h electrolysis using ion chromatogram and indophenol blue method, respectively.

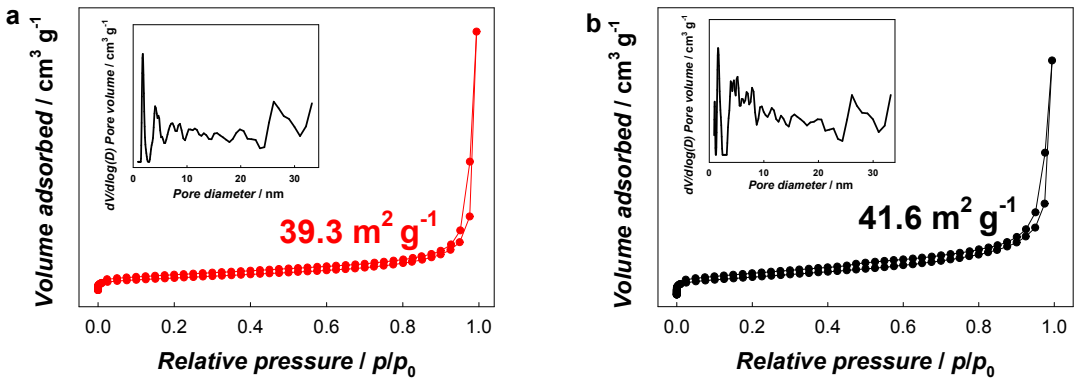

Fig. S9 Nitrogen adsorption/desorption isotherm curves and their corresponding pore size distributions (inset) of (a) Fe-MnO_2 and (b) MnO_2.

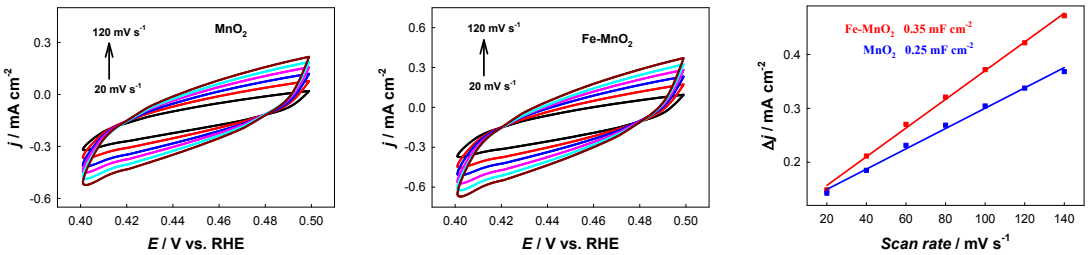

Fig. S10. CV curves (a) MnO_2/CP and (b) Fe-MnO_2/CP. (c) The capacitive currents at –0.45 V vs. RHE as a function of scan rates for MnO_2/CP and Fe-MnO_2/CP.

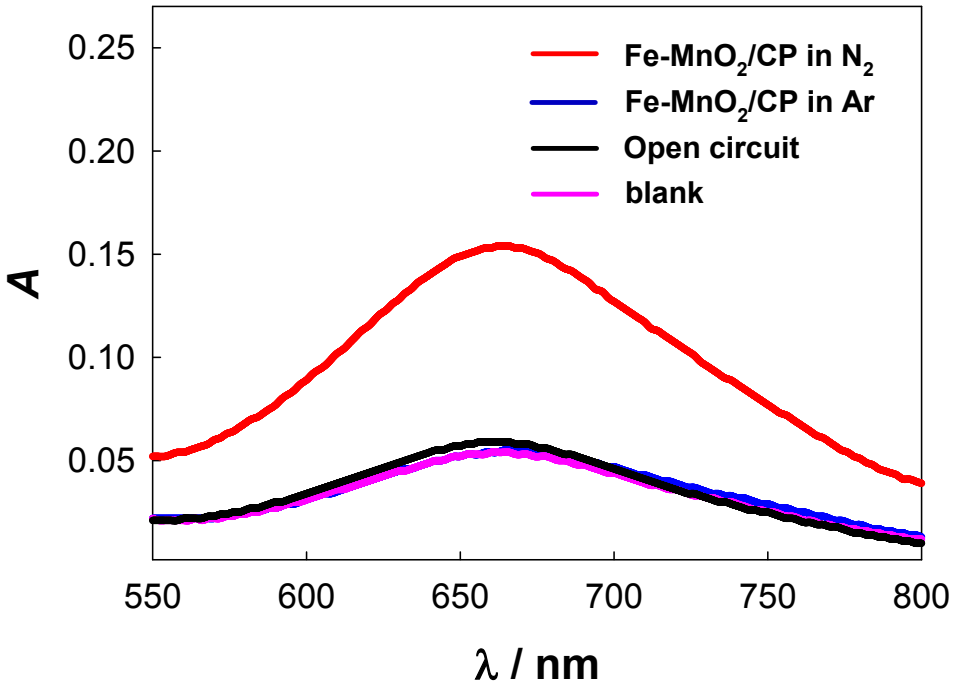

Fig. S11 UV-Vis absorption spectra of the electrolytes stained with indophenol indicator after 2 h electrolysis under different conditions:–0.29 V in N_2-saturated electrolyte, –0.29 V in Ar-saturated electrolyte, open circuit in N_2-saturated electrolyte, and blank.

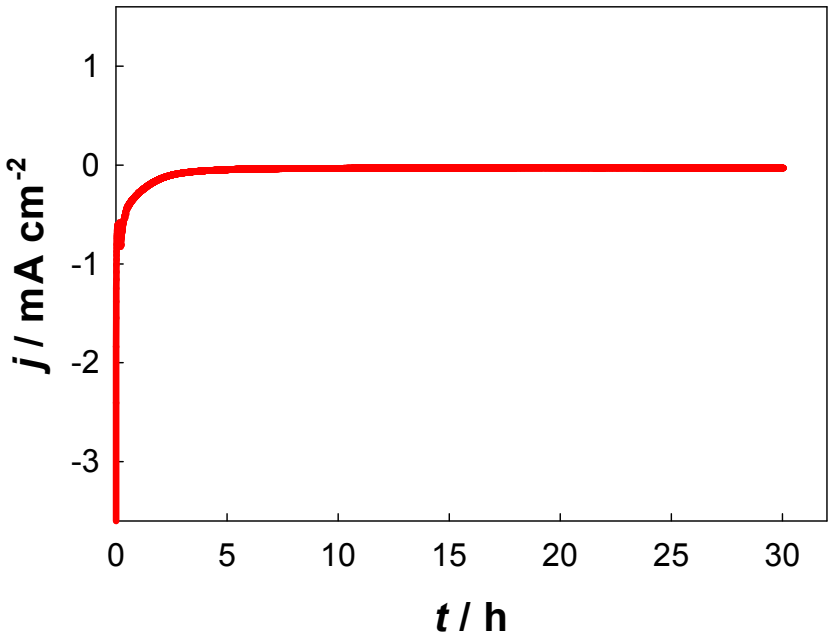

Fig. S12 Chronoamperometry curve at -0.29 V using Fe-MnO_2/CP catalyst (30 h).

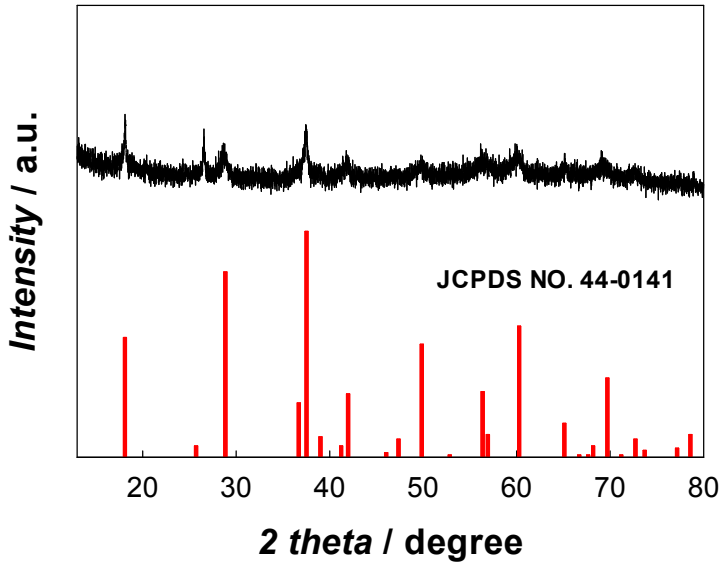

Fig. S13 XRD patterns of Fe-MnO_2 after stability test in N_2-saturated solution.

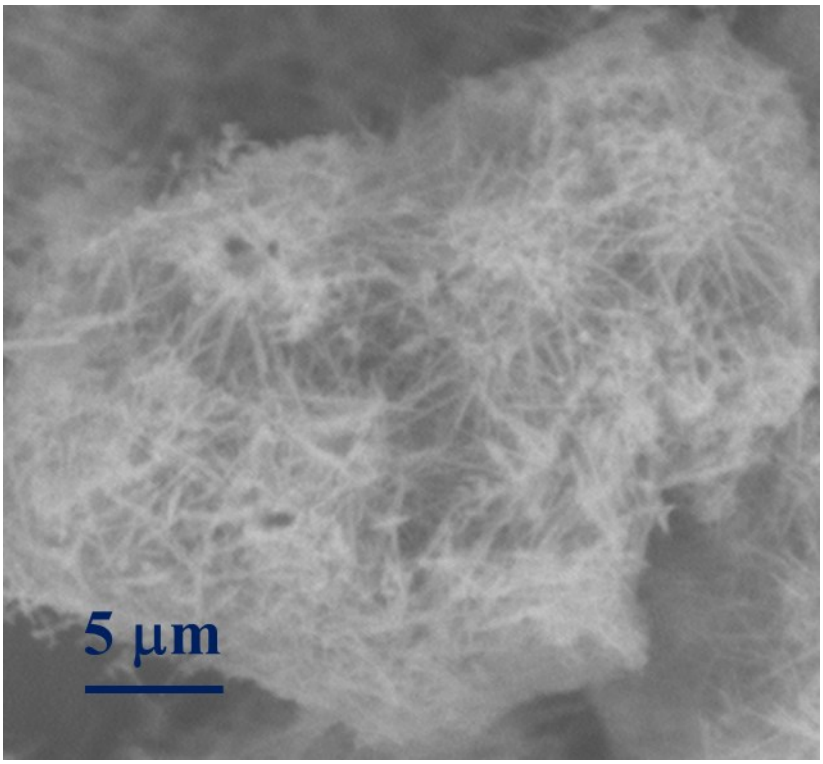

Fig. S14 SEM image of Fe-MnO_2 after stability test in N_2-saturated solution.

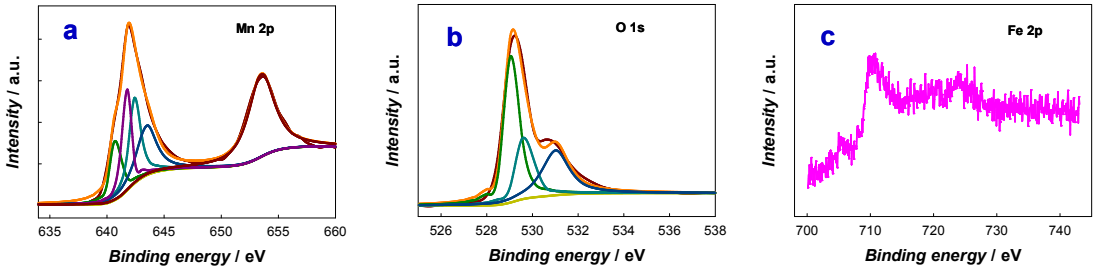

Fig. S15 The XPS of Mn 2p (a), O 1s (b) and Fe 2p (c) regions for Fe-MnO_2 after stability test in N_2-saturated solution. The XPS results in (a)-(c) also suggest that stability did not make much change on the chemical state of Mn, O and Fe.

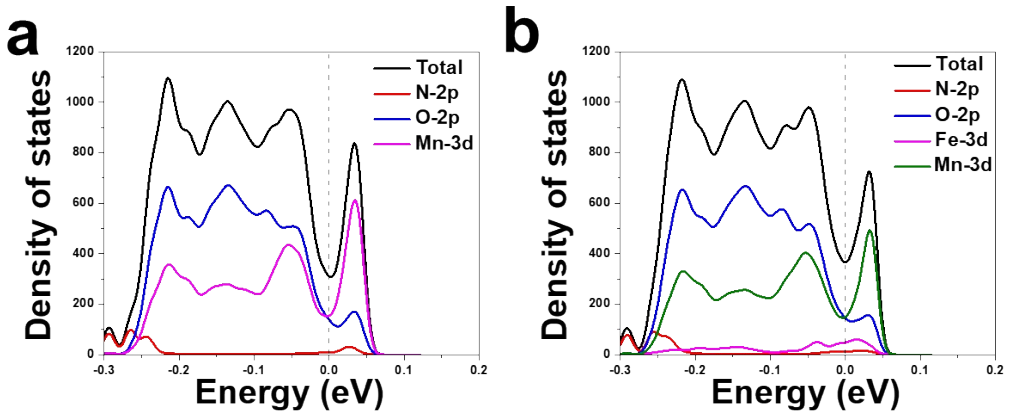

Fig. S16 Density of states of the N_2 adsorption on (211) surface of (a) MnO_2 and (b) Fe-MnO_2 for side-on configurations. The vertical dashed lines denote the Fermi energy.

Table S1 ICP analysis of Fe in the electrolyte.

Time （h）	2
Concentration of Fe (ppm)	0.003

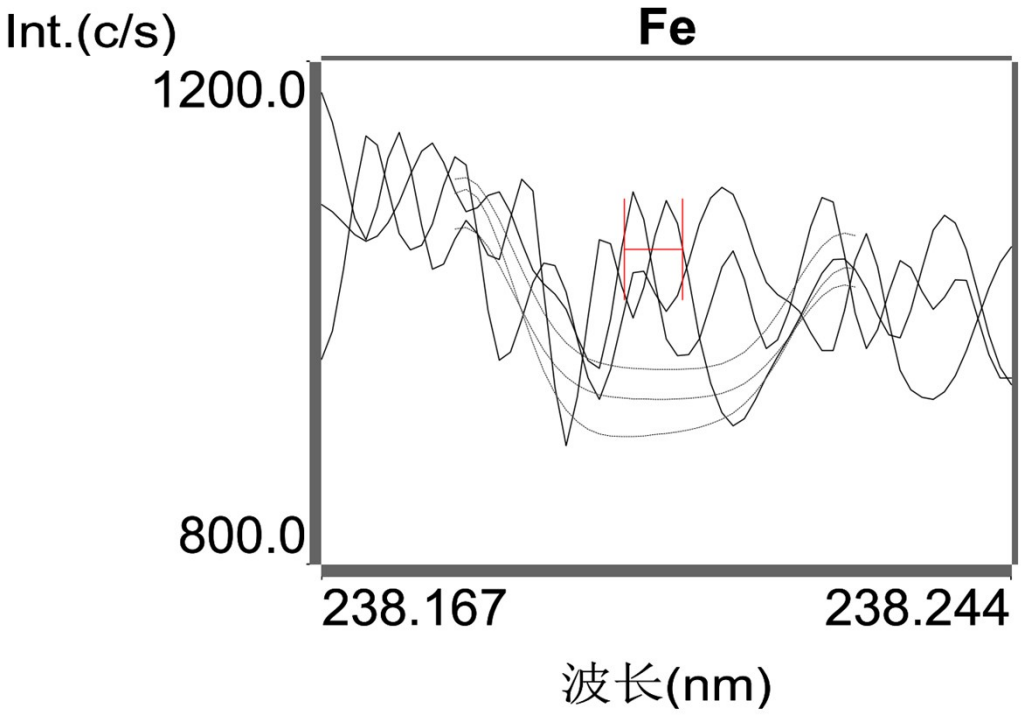

The ICP-OES measurement is used to detect the concentration of Fe in the electrolyte after 2 h electrolysis. According to the ICP-OES analysis results, the concentration of Fe in the electrolyte is 0.003 ppm after 2 h electrolysis. This result demonstrates the high structural stability of the catalyst during the electrochemical process.

Table S1 Summary of the representative reports on electrocatalytic N_2 fixation at ambient conditions.

Catalysts	Electrolytes	NH_3 yield	Faradaic efficiency	References
Fe-MnO_2	**0.1 M Na_2SO_4**	**39.2 μg h^{-1} $mg_{cat.}^{-1}$ 2.56×10^{-10} mol s^{-1} cm^{-2}**	**16.8%**	**This work**
Mn_3O_4	0.1 M Na_2SO_4	11.6 μg h^{-1} $mg_{cat.}^{-1}$	3%	[6]
MnO	0.1 M Na_2SO_4	7.92 μg h^{-1} $mg_{cat.}^{-1}$	8.02%	[7]
MnO_x	0.1 M Na_2SO_4	1.63×10^{-10} mol s^{-1} cm^{-2}	11.4%	[8]
Mn_3O_4@rGO	0.1 M Na_2SO_4	17.4 μg h^{-1} $mg_{cat.}^{-1}$	3.52%	[9]
MnO_2-$Ti_3C_2T_x$	0.1 M HCl	34.12 μg h^{-1} $mg_{cat.}^{-1}$	11.39%	[10]
$LiMnO_4$	0.1 M HCl	15.83 μg h^{-1} $mg_{cat.}^{-1}$	7.44%	[11]
NaOH–$Ti_3C_2T_x$	0.1 M HCl	36.9 μg h^{-1} $mg_{cat.}^{-1}$	9.1%	[12]
$WO_{3-x}(V_o)\_H_2$	0.1 M HCl	4.2 μg h^{-1} $mg_{cat.}^{-1}$	6.8%	[13]
WO_3	0.1 M HCl	17.28 μg h^{-1} $mg_{cat.}^{-1}$	7.0%	[14]
Au Nanorod	0.1 M KOH	6.042 μg h^{-1} $mg_{cat.}^{-1}$	3.879%	[15]
Rh nanosheets	0.1 M KOH	23.88 μg h^{-1} $mg_{cat.}^{-1}$	0.217%	[16]
Mo_2C	0.5 M Li_2SO_4	11.3 μg h^{-1} $mg_{cat.}^{-1}$	7.8%	[17]
Cu/AC-S	0.1 M Na_2SO_4	9.7μg h^{-1} $mg_{cat.}^{-1}$	15.9%	[18]
$BiVO_4$	0.2 M Na_2SO_4	8.6 μg h^{-1} $mg_{cat.}^{-1}$	10.04%	[19]
Bi NS	0.1 M Na_2SO_4	13.23 μg h^{-1} $mg_{cat.}^{-1}$	10.49%	[20]
Defect-rich MoS_2	0.1 M Na_2SO_4	2.93 μg h^{-1} $mg_{cat.}^{-1}$	8.34%	[21]
FeN_4	0.1 M Na_2SO_4	10.25 μg h^{-1} $mg_{cat.}^{-1}$	14.17	[22]

References

1. L. Xia, X. Wu, Y. Wang, Z. Niu, Q. Liu, T. Li, X. Shi, A. M. Asiri and X. Sun, *Small Methods*, 2019, **3**, 1800251-1800256.
2. P. Li, J. Wang, H. Chen, X. Sun, J. You, S. Liu, Y. Zhang, M. Liu, X. Niu and Y. Luo, *J. Mater. Chem. A*, 2019, **7**, 12446-12450.
3. B. Delley, *J. Chem. Phys.*, 1990, **92**, 508-517.
4. J. P. Perdew, K. Burke and M. Ernzerhof, *Phys. Rev. Lett.*, 1996, **77**, 3865.
5. B. Delley, *J. Chem. Phys.*, 2000, **113**, 7756-7764.
6. X. Wu, L. Xia, Y. Wang, W. Lu, Q. Liu, X. Shi and X. Sun, *Small*, 2018, **14**.
7. Z. Wang, F. Gong, L. Zhang, R. Wang, L. Ji, Q. Liu, Y. Luo, H. Guo, Y. Li and P. Gao, *Adv. Sci.*, 2019, **6**, 1801182-1801190.
8. L. Zhang, X. Y. Xie, H. Wang, L. Ji, Y. Zhang, H. Chen, T. Li, Y. Luo, G. Cui and X. Sun, *Chem. Commun.*, 2019, **55**, 4627-4630.
9. H. Huang, F. Gong, Y. Wang, H. Wang, X. Wu, W. Lu, R. Zhao, H. Chen, X. Shi, A. M. Asiri, T. Li, Q. Liu and X. Sun, *Nano Research*, 2019, **12**, 1093-1098.
10. W. Kong, F. Gong, Q. Zhou, G. Yu, L. Ji, X. Sun, A. M. Asiri, T. Wang, Y. Luo and Y. Xu, *J. Mater. Chem. A*, 2019.
11. C. Li, J. Yu, L. Yang, J. Zhao, W. Kong, T. Wang, A. M. Asiri, Q. Li and X. Sun, *Inorg. Chem.*, 2019, **58**, 9597-9601.
12. T. Li, L. Yao, Q. Liu, J. Gu, R. Luo, J. Li, X. Yan, W. Wang, P. Liu and B. Chen, *Angew. Chem., Int. Ed.*, 2018, **7**, 14462-14465.
13. Z. Sun, R. Huo, C. Choi, S. Hong, T.-S. Wu, J. Qiu, C. Yan, Z. Han, Y. Liu and Y.-L. Soo, *Nano Energy*, 2019, 869-875.
14. W. Kong, R. Zhang, X. Zhang, L. Ji, G. Yu, T. Wang, Y. Luo, X. Shi, Y. Xu and X. Sun, *Nanoscale*, 2019, 1-4.
15. D. Bao, Q. Zhang, F. L. Meng, H. X. Zhong, M. M. Shi, Y. Zhang, J. M. Yan, Q. Jiang and X. B. Zhang, *Adv. Mater.* , 2017, **29**, 1604799-1604804.
16. H.-M. Liu, S.-H. Han, Y. Zhao, Y.-Y. Zhu, X.-L. Tian, J.-H. Zeng, J.-X. Jiang, B. Y. Xia and Y. Chen, *J. Mater. Chem. A*, 2018, **6**, 3211-3217.
17. H. Cheng, L. X. Ding, G. F. Chen, L. Zhang, J. Xue and H. Wang, *Adv. Mater.*, 2018, **30**, 1803694-1803671.
18. S. Zhang, W. Li, Y. Liu, J. Wang and H. Zhang, *Inorg. Chem. Front.*, 2019, **6**, 2832-2836.
19. J. X. Yao, D. Bao, Q. Zhang, M. M. Shi, Y. Wang, R. Gao, J. M. Yan and Q. Jiang, *Small Methods*, 2018, **6**, 1800333-1800342.
20. L. Li, C. Tang, B. Xia, H. Jin, Y. Zheng and S.-Z. Qiao, *ACS Catal.*, 2019, **9**, 2902-2908.
21. J. Xie, H. Zhang, S. Li, R. Wang, X. Sun, M. Zhou, J. Zhou, X. W. Lou and Y. Xie, *Adv. Mater.* , 2013, **25**, 5807-5813.
22. C. He, Z.-Y. Wu, L. Zhao, M. Ming, Y. Zhang, Y. Yi and J.-S. Hu, *ACS Catal.*, 2019, **9**, 7311-7317.